Optimization of nonlinear, non-Gaussian Bayesian filtering for diagnosis and prognosis of monotonic degradation processes

Matteo Corbetta [a], Claudio Sbarufatti [a,*], Marco Giglio [a], Michael D. Todd [b]

[a] *Politecnico di Milano, Dipartimento di Meccanica, Milan, Italy*
[b] *University of California San Diego, Department of Structural Engineering, San Diego, CA, United States*

The present work critically analyzes the probabilistic definition of dynamic state-space models subject to Bayesian filters used for monitoring and predicting monotonic degradation processes. The study focuses on the selection of the random process, often called *process noise*, which is a key perturbation source in the evolution equation of particle filtering. Despite the large number of applications of particle filtering predicting structural degradation, the adequacy of the picked process noise has not been investigated. This paper reviews existing process noise models that are typically embedded in particle filters dedicated to monitoring and predicting structural damage caused by fatigue, which is mono-tonic in nature. The analysis emphasizes that existing formulations of the process noise can jeopardize the performance of the filter in terms of state estimation and remaining life prediction (i.e., damage prognosis). This paper subsequently proposes an optimal and unbiased process noise model and a list of requirements that the stochastic model must satisfy to guarantee high prognostic performance. These requirements are useful for future and further implementations of particle filtering for monotonic system dynamics. The validity of the new process noise formulation is assessed against experimental fatigue crack growth data from a full-scale aeronautical structure using dedicated performance metrics.

1. Introduction

Bayesian filtering algorithms are gaining popularity in many engineering applications and they are emerging as a state-of-the-art technique in the fields of probabilistic life prediction, structural health monitoring (SHM), and prognostics and health management (PHM), especially when the diagnostic-prognostic process requires real-time execution. Among the dif-ferent classes of Bayesian filters, particle filtering, a sequential Monte Carlo method developed by Gordon, Salmond and Smith [1], is of great interest because of its ability to deal with nonlinear systems characterized by non-Gaussian variables [1–6]. Recent applications of particle filtering have been presented in literature in a number of diagnostic and prognostic scenarios: fault detection in structural components [7,8], prediction of turbine blade creep [9], prediction of lithiumion battery degradation [10,11] and asymptotic process prediction in composite materials [12]. Literature also provides examples of particle filtering applied in the field of nonlinear structural dynamics and structural parameter identification [13,14]. Other works related to particle filtering are analyzed throughout the paper.

∗ Corresponding author.
E-mail address: claudio.sbarufatti@polimi.it (C. Sbarufatti).

Nomenclature

C^*	Paris' law parameter
F	crack shape function
K	stress intensity factor
k	discrete time step
k^*	gamma distribution parameter
N	load cycle
N_s	number of samples
n	system state vector dimension
m	measurement vector dimension
m^*	Paris' law parameter
p	input vector dimension
q	model parameter vector dimension
S	remote stress
$\mathcal{U}$	input vector support
$\boldsymbol{u}$	input vector
$\mathcal{X}$	system state vector support
$\boldsymbol{x}$	system state vector
$\mathcal{Z}$	measurement vector support
$\boldsymbol{z}$	observation vector
$\delta_{..}$	Kronecker delta
$\boldsymbol{H}$	measurement noise vector support
$\boldsymbol{\eta}$	measurement noise
Θ	model parameter vector support
θ^*	gamma distribution parameter
θ	model parameter vector
μ	mean
Σ	covariance matrix
σ	standard deviation
σ^2	variance
Ω	process noise vector support
$\boldsymbol{\omega}$	process noise vector

The design of the filter includes a random process introduced in the model equation describing the system dynamics. This random process works as a perturbation source describing the inherent, un-modeled uncertainty of the system and is inherent in defining the probability density function (pdf) of the system state variables. Such process noise aims at describing, for example, micro-scale dynamics of the damaging process, which is not accounted for in macro-scale engineering models. In the fields of SHM and PHM, such a random process is often called *process noise*, where the term 'process' indicates the system evolution process, and 'noise' emphasizes its stochastic, perturbative nature. The definition of the process noise is typically made by the algorithm designer, but none of the applications of particle filtering for diagnostic and prognostic of structures presented in literature discusses the efficiency and effectiveness of the chosen random process. This paper will clearly show that this selection does, in fact, have implications on the filter's predictive performance.

In addition to the above-cited papers [7–11], the works in [15–20] are remarkable examples of real-time fatigue crack growth (FCG) prognosis in metallic structures based on particle filtering. Recent works investigating different aspects of particle filtering-based FCG prognosis are also available in [21–23]. Applications of particle filtering for life prediction of composite materials subject to matrix micro-cracking are available in [12,24,25]. All those papers defined the process noise in different ways (some of them using nonlinear non-Gaussian random processes), but none of them discussed the selected process critically.

The analysis presented in this paper shows that if the process noise is not carefully tuned, the algorithm may encounter computational inefficiencies or it might fail the prognostic goal, defined here to be the accurate prediction of the remaining useful life (RUL) of the structure. Indeed, this analysis shows the drawbacks of process noises adopted in previous papers. Then, the paper proposes a process noise to improve the efficiency and effectiveness of particle filtering for monitoring and prognosis of monotonic degradation phenomena. Cracks in metallic alloys, delamination and matrix crack density evo-lution in composite laminates, and creep-induced plasticity are typical cases of monotonic degradation where particle filter-ing (if properly tuned) can help in monitoring the damage severity and predicting the RUL. It should be noted that the proposed process noise was already used by the authors in an application of particle filtering for composite materials suf-fering concurrent damage mechanisms [26]. Nevertheless, a critical analysis of the process noise was not presented in that work. Also, this paper proposes three requirements that the evolution equation, which strongly depends on the process noise, has to satisfy in order to build an efficient Bayesian filtering framework. Eventually, the designed filter is applied

to FCG observed in a real helicopter tail and the results are compared with older algorithm formulations available in literature based on well-known evaluation metrics. This application is a relevant example of particle filtering-based damage prognosis applied to a real aeronautical structure.

The remainder of the paper organizes as follows: Section 2 summarizes particle filtering, the system state refinement and the prognostic step to predict the evolution of the (monotonic) degradation process. Section 3 analyzes the evolution equation tailored for monotonic processes and the effect of the process noise. This section discusses also the requirements of the evolution equation to design an effective particle filter. Section 4 shows the application to FCG data obtained in a lab environment and Section 5 concludes the paper.

2. Summary of particle filtering for nonlinear non-Gaussian system tracking

Particle filtering is a Bayesian filtering technique relying upon Monte Carlo importance sampling to approximate the conditional pdf of the system state [2,3]. The recursive filtering of the system state acts upon a dynamic state-space model, which is composed of an evolution equation describing the system dynamics and an observation equation that links the observables, i.e., what is measured, with the true (unknown, and possibly hidden) system state. The dynamic state-space model is described by a first-order Markov assumption (1):

$$
\begin{aligned}
\mathbf{x}_k &= f_{k,\theta}(\mathbf{x}_{k-1}, \mathbf{u}_{k-1}, \boldsymbol{\omega}_{k-1}) \\
\mathbf{z}_k &= g_k(\mathbf{x}_k, \boldsymbol{\eta}_k),
\end{aligned}
\tag{1}
$$

where the vector $\mathbf{x} = [x_1, x_2, \ldots, x_n]^T \subseteq \mathcal{X} \in \mathbb{R}^{n \times 1}$ contains the n state variables, while the vector $\mathbf{z} = [z_1, z_2, \ldots, z_m]^T \subseteq \mathcal{Z} \in \mathbb{R}^{m \times 1}$ contains the m observations. The evolution equation is defined by $f_{k,\theta}(\cdot)$, which is an n-dimensional state mapping function parametrized by the model parameter vector $\theta = [\theta_1, \theta_2, \ldots, \theta_q]^T \subseteq \Theta \in \mathbb{R}^{q \times 1}$, while $g_k(\cdot)$ is a m-dimensional mapping function defining the observation equation. Both $f_{k,\theta}(\cdot)$ and $g_k(\cdot)$ are nonlinear and potentially time-varying. The two random processes $\boldsymbol{\omega}_{k-1} \subseteq \Omega \in \mathbb{R}^{n \times 1}$ and $\boldsymbol{\eta}_k \subseteq H \in \mathbb{R}^{m \times 1}$ are the process and measurement noise, respectively. They contribute to the evolution and observation equations by adding random perturbations. As explained in the introduction, the process noise introduces a disturbance to account for the inherent, unpredictable variability in the system dynamics, and is the core of the discussion in Section 3. The measurement noise describes the uncertainty of the measurement system, and can be easily quantified when a series of repeatable observations is available. Although some authors defined them as white noise processes [27], they can be general first-order random processes with time-varying moments.

A common assumption is that the input of the system $\mathbf{u} = [u_1, u_2, \ldots, u_p]^T \in \mathcal{U} \subseteq \mathbb{R}^{p \times 1}$ is observable, and its observability is not further discussed henceforth. Unless otherwise specified, the model parameter vector and the input vector are supposed to be deterministic and known. Thus, the dependence from the input vector is not underlined in the following equations. Also, dissertations on the observation equation, including frequency of observations and observation uncertainty, are not provided, since the paper focuses on the noise affecting the evolution equation only. With an abuse of notation, the distinction between random variables or random vectors and their realizations is also neglected. Since detailed discussions on particle filtering are not the aim of the paper, however, the interested reader may refer to [1–6] for more details.

2.1. Filtering of the dynamic state-space model

The filtering problem aims at estimating the conditional pdf of the system state upon the observation sequence $\mathbf{z}_{0:k}$, and its closed form solution consists of the Chapman-Kolmogorov equation (*prediction*) and the *Bayesian updating* (2)

$$
\begin{aligned}
p(\mathbf{x}_k | \mathbf{z}_{0:k-1}) &= \int_{\mathcal{X}} p(\mathbf{x}_k | \mathbf{x}_{k-1}) p(\mathbf{x}_{k-1} | \mathbf{z}_{0:k-1}) \mathrm{d}\mathbf{x}_{k-1}, \\
p(\mathbf{x}_k | \mathbf{z}_{0:k}) &= \frac{p(\mathbf{x}_k | \mathbf{z}_{0:k-1}) p(\mathbf{z}_k | \mathbf{x}_k)}{p(\mathbf{z}_k | \mathbf{z}_{0:k-1})}.
\end{aligned}
\tag{2}
$$

Since the evolution of $\mathbf{x}$ undergoes to the assumption of first-order Markov processes (first row of (1)), the prediction equation has made use of the fact that $p(\mathbf{x}_k | \mathbf{x}_{k-1}, \mathbf{z}_{0:k-1}) = p(\mathbf{x}_k | \mathbf{x}_{k-1})$, [3]. The analytical solution of (2) exists for linear-Gaussian systems only. On the other hand, particle filter enables the approximation of the posterior pdf of a nonlinear non-Gaussian system state given a series of observations, $p(\mathbf{x}_k | \mathbf{z}_{0:k})$, by means of N_s samples $\mathbf{x}_k^{(i)}$, $i = 1, \ldots, N_s$. These samples are often called *particles*, weighted using the importance sampling approach (3), [3]. The weights are normalized to sum up to 1 (4) before computing the posterior distribution (5),

$$
\tilde{w}_k^{(i)} = w_{k-1}^{(i)} \frac{p(\mathbf{z}_k | \mathbf{x}_k^{(i)}) p(\mathbf{x}_k^{(i)} | \mathbf{x}_{k-1}^{(i)})}{q(\mathbf{x}_k^{(i)} | \mathbf{x}_{k-1}^{(i)}, \mathbf{z}_{0:k})},
\tag{3}
$$

$$
w_k^{(i)} = \frac{\tilde{w}_k^{(i)}}{\sum_{j=1}^{N_s} \tilde{w}_k^{(j)}},
\tag{4}
$$

$$\hat{p}(\boldsymbol{x}_k|\boldsymbol{z}_{0:k}) = \sum_{i=1}^{N_s} w_k^{(i)} \delta_{\boldsymbol{x}_k^{(i)},\boldsymbol{x}_k} \tag{5}$$

The functions in (3) are the *transition density function* (tdf), $p(\boldsymbol{x}_k|\boldsymbol{x}_{k-1})$, the *likelihood function*, $p(\boldsymbol{z}_k|\boldsymbol{x}_k)$ and the *importance density function*, $q(\boldsymbol{x}_k|\boldsymbol{x}_{k-1},\boldsymbol{z}_{0:k})$. The choice of the importance density function is arbitrary, and a common practice is to use the tdf as the importance density function, thus simplifying the weight formulation (6),

$$\tilde{w}_k^{(i)} = w_{k-1}^{(i)} p(\boldsymbol{z}_k|\boldsymbol{x}_k^{(i)}). \tag{6}$$

The evolution equation $f_{k,\theta}(\cdot)$ is the core of the tdf and is analyzed in Section 3. The algorithm based on Eqs. (4)–(6) is called *bootstrap* sequential importance sampling or bootstrap particle filter and is the most common algorithm adopted in real-time diagnostic and prognostic applications, although some applications of auxiliary particle filter for structural state diagnosis can be found in literature [7].

2.2. Prognostics: from the state refinement to the p-step ahead prediction

Particle filtering approximates the posterior distribution of the system state, which is a state estimation-refinement rather than a prognosis [27]. The prognostic stage is carried out by projecting the samples ahead into the future, at time step p, using the evolution equation $f_{k,\theta}(\cdot)$, (i.e., $p(\boldsymbol{x}_k|\boldsymbol{x}_{k-1})$). The prognostic step makes use of the pdfs defined in SubSection 2.1 and approximates the *p-step ahead prediction distribution* (7), as defined by Doucet, Godsill and Andrieu [2],

$$\hat{p}(\boldsymbol{x}_{k+p}|\boldsymbol{z}_{0:k}) = \sum_{i=1}^{N_s} w_k^{(i)} \int_{\mathcal{X}} p\left(\boldsymbol{x}_{k+1}|\boldsymbol{x}_k^{(i)}\right) \prod_{j=k+2}^{k+p} p(\boldsymbol{x}_j|\boldsymbol{x}_{j-1}) \, \mathrm{d}\boldsymbol{x}_{k+1:k+p-1}. \tag{7}$$

The estimation of the end-of-life or the RUL of systems subject to progressive degradation involves the step-by-step propagation of the samples $\boldsymbol{x}_k^{(i)}$ using the tdf. Once all the samples have crossed a predefined threshold $\boldsymbol{x}_{th}$ defining a critical or limit degradation, the RUL pdf may be computed using (8),

$$\hat{p}(\mathrm{RUL}_k|\boldsymbol{z}_{0:k}) = \sum_{i=1}^{N_s} w_k^{(i)} \delta_{\mathrm{RUL}_k^{(i)},\mathrm{RUL}_k}. \tag{8}$$

The term $\mathrm{RUL}_k^{(i)}$ is the remaining life of the *i-th* sample, i.e., the time required by $\boldsymbol{x}_k^{(i)}$ to reach $\boldsymbol{x}_{th}$, evaluated with the information up to time step k.

3. On the probabilistic transition using the process noise ω

This section analyzes the tdf $p(\boldsymbol{x}_k|\boldsymbol{x}_{k-1})$ and the effect of the selected process noise to the transition of the samples. Assuming that $f_{k,\theta}(\cdot)$ is not time-varying (i.e., $f_{k,\theta}(\cdot) \equiv f_\theta(\cdot)$), the process noise ω is the only source of uncertainty affecting the transition of the *i-th* sample. In addition, the features of the process noise have been assumed as stationary; ω loses indeed the dependence from the time step k (9):

$$f_\theta(\boldsymbol{x}_{k-1},\omega) \rightarrow p(\boldsymbol{x}_k|\boldsymbol{x}_{k-1}). \tag{9}$$

Each sample of the system state must perform a 'plausible' transition from $\boldsymbol{x}_{k-1}^{(i)}$ to $\boldsymbol{x}_k^{(i)}$ in the state-space, in agreement with the true, physical phenomenon. The requirements to generate likely transitions to monitor monotonic degradation processes are discussed below, including: (i) the use of additive Gaussian or non-Gaussian and (ii) multiplicative log-normal process noises adopted in the literature.[1] Then, a process noise definition and a list of requirements necessary to implement an efficient filter are discussed. Without loss of generality, the system's state has been considered unidimensional, $x_k \subseteq \mathcal{X} \in \mathbb{R}$, and the analysis of the evolution equation has made use of the algebra of random variables.

3.1. Additive Gaussian/non-Gaussian process noises

The works in [12,15,18,24,25], concerning fatigue-induced damage prognosis, proposed an additive noise altering the evolution equation, (10),

$$x_k = f'_\theta(x_{k-1}) + \omega. \tag{10}$$

The nonlinear function f'_θ is the deterministic evolution equation, which describes the system state dynamics without any perturbation source. The superscript $\prime$ is used to differ the deterministic model and the stochastic evolution function $f_\theta(x_{k-1},\omega)$. A simple analysis of the evolution equation in (10) can be carried out by using the conditional expectation of the system state (11):

---

[1] The notation of the original papers has been modified to make it consistent with the notation used in this work.

$$E[x_k|x_{k-1}] = f'_\theta(x_{k-1}) + E[\omega]. \tag{11}$$

Assuming a Gaussian process noise, the tdf describing the probability of $x_k^{(i)}$ given $x_{k-1}^{(i)}$ is a Gaussian distribution (12):

$$p(x_k|x_{k-1}) = \frac{1}{\sqrt{2\pi}\sigma_\omega} \exp\left(-\frac{(x_k - E[x_k|x_{k-1}])^2}{\sigma_\omega^2}\right). \tag{12}$$

Clearly, the expected value of the system state is unbiased only if $E[\omega] = 0$. The work in [15] assumes ω as a non-Gaussian random process, but further details were not provided. In [18], the authors used two types of process noise in an illustrative example: a Gamma distribution, $\omega \sim \Gamma(0.15, 0.3)$, and a Normal distribution $\omega \sim \mathcal{N}(0.045, 0.1162)$. Later in their paper, they applied the filter to experimental data using a 'non-Gaussian white noise', without further information. Instead, the authors in [12,24,25] used Eq. (10) with a zero-mean Gaussian random process.

If the one-step ahead prediction is biased ($E[x_k|x_{k-1}] \neq f'_\theta(x_{k-1})$), the discrepancy between the deterministic evolution equation and the prediction made by the filter increases with the horizon of the prediction, altering the trend of the particles. The bias becomes larger and larger when projecting the samples several steps ahead in the future, so it could produce notable effects in the prognostic stage. Some authors adopted a non-zero-mean noise to adjust the evolution equation using historical data. However, such data may not be available for the system or structure that has to be monitored. Also, if historical damage propagation data suggest that there is a bias with respect to the models available in literature, such data could be efficiently used to modify the model parameters, so that the model would fit those historical data correctly. Table 1 summarizes the additive process noises for structural degradation found in the literature.

Even though zero-mean Gaussian random processes will not introduce biases into the evolution equation, they may let the samples fall outside the domain support of the system state, i.e., a domain support mismatch. Let us assume an additive Gaussian process noise and consider the system state x_k as the size of a fatigue-induced damage: crack length, delamination extent, etc. The domain of existence of the state vector is the positive sub-set of real numbers, $\mathcal{X} \in \mathbb{R}_{[0,\infty]}$. The use of a Gaussian process noise allows the sample $x_k^{(i)}$ to be smaller that $x_{k-1}^{(i)}$, because of the symmetry of the Gaussian distribution. If the sample decreases for a relatively large number of steps, it might become less than zero, and the algorithm fails, without providing any RUL estimation. As a matter of fact, a decreasing system state is not consistent with damage progression phenomena, since aging or fatigue damage accumulates as time passes by, i.e., monotonically increases.

In order to give a clear, graphical explanation of the effect of the process noise on the particles' propagation, $N_s = 100$ samples of FCG have been propagated for $N = 150,000$ load cycles using (10) and process noises similar to the one found in literature (Table 1). This simulation refers to a virtual aluminum plate with a central crack, and the simulation features are available in Table 2. A linear damage accumulation model based on Paris' law simulates the step-by-step damage progression (13):

$$x_k = x_{k-1} + C^*(\Delta K(x_{k-1}))^{m^*} \Delta N + \omega. \tag{13}$$

The stress intensity factor range is the difference between the maximum and minimum stress intensity factors within a single load cycle, $\Delta K = K(S_{max}) - K(S_{min})$, and $\Delta N = 200$. The samples, each of them referring to a specific crack length, are projected in the future for several time steps (or load cycles) using (13). This simulation is representative of the particle filtering-based prognostic stage, when the posterior pdf of the system state has been already computed and there is no additional information regarding the true damage progression.

Fig. 1 shows the Monte Carlo simulation compared with a Paris' law-based deterministic model. The noise generated from a zero-mean Gaussian distribution (Fig. 1a) keeps the samples centered on the deterministic model, i.e., $E[x_k|x_{k-1}] = f'_\theta(x_{k-1}), \forall k \in \mathbb{N}$. However, if the process noise variance was too large, a sample propagation would unlikely represent a FCG progression. The samples in Fig. 1a make large jumps at every step, and some of them become negative ($x_k^{(i)} < 0$). It is difficult to identify a crack growth path because of the large perturbation caused by the noise. The reduction of the process noise variance would solve the problem, but two main issues arise. Firstly, the closeness of the damage size to zero would affect the selection of σ_ω^2. As a matter of fact, the closer the damage is to zero, the higher the probability of the samples that will fall below zero, because of the symmetric nature of the Gaussian distribution. As a consequence, the choice

Table 1
Additive noise already used in particle filters for prognosis. The last column is the bias introduced in a single step: from k-1 to k. (σ_ω^2 indicates that the original papers did not provide the value of the process noise variance).

Paper	System state	Random process ω	$E[\omega]$
[18]	Crack length	$\sim \Gamma(0.15, 0.3)$	0.045, mm
	Crack length	$\sim \mathcal{N}(0.045, 0.1162)$	0.045, mm
[24]	Matrix crack density	$\sim \mathcal{N}(0, \sigma_\omega^2)$	0, #/m
[25]	Matrix crack density, stiffness	$\sim \mathcal{N}(0, 4)$	0, #/m
[12]	Matrix crack density, stiffness, reliability	$\sim \mathcal{N}(0, \sigma_\omega^2)$	0, #/m

Table 2

FCG simulation features.

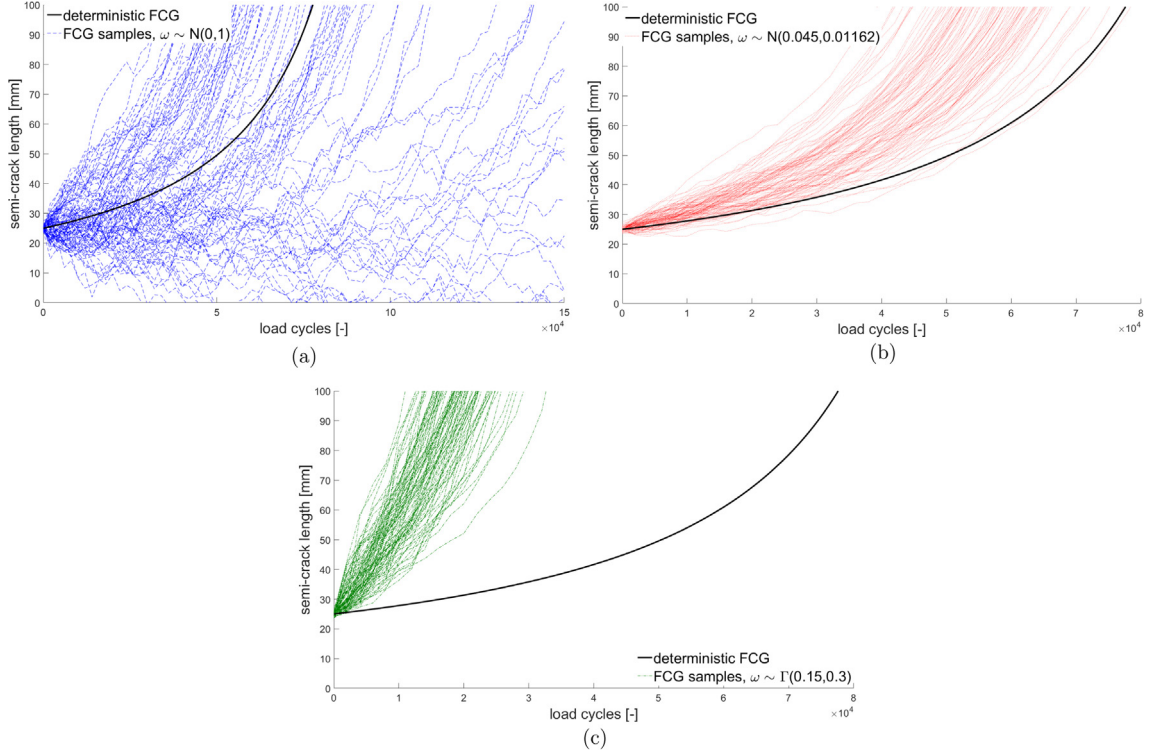|	
Virtual structure	Infinite Aluminum plate Al2024
Damage	Central, through-the-thickness crack
Crack shape function	$F = 1$
Applied fatigue stress	$\Delta S = 60$ MPa
Damage feature	Stress intensity factor $K = FS\sqrt{x\pi}$
FCG model	Paris' law $C^*(\Delta K)^{m^*}$
Paris' law parameters	$C^* = 1.1994e - 14, \ m^* = 3.79$
Initial semi-crack length pdf	$\mathcal{N}(25, 0.5)$

Fig. 1. Monte Carlo samples of FCG starting from a known initial distribution. The different process noises can generate unlikely damage progression paths (a), or biases of the sample swarm (b-c) that can jeopardize the efficiency of the algorithm.

of σ_ω^2 would change on a case-by-case basis. Secondly, a too small of a process noise variance would neglect the randomization effect caused by ω. Particle filters may still work with null process noise, though the algorithm would neglect the presence of non-modeled phenomena of the damage progression, assuming that the model underneath the filter is 'correct'. The other process noises introduce a bias in the evolution equation, and this bias increases with the number of simulation steps (Fig. 1b and c). The additive Gaussian noise in 1b seems to keep the particles in the correct region (positive domain), thanks also to the bias. However, the initial crack length (~ 25mm) is relatively large, and a smaller initial crack size might generate the same problem seen in Fig. 1a. The bias introduced by the Gamma process noise is very large; all of the samples have a trend that is significantly different from the deterministic equation. As a consequence, the use of an additive Gaussian (or non-Gaussian) process noise is not considered optimal for monotonic degradation processes.

3.2. Multiplicative log-normal process noises

Another process noise formulation for FCG prognosis was proposed by Cadini, Zio, Avram [19] by referring to [28]. They used a log-normal random process $e^\omega, \omega \sim \mathcal{N}(\mu_\omega = 0, \ \sigma_\omega^2)$ multiplied to the deterministic FCG rate (14), assuming $\Delta N = 1$,

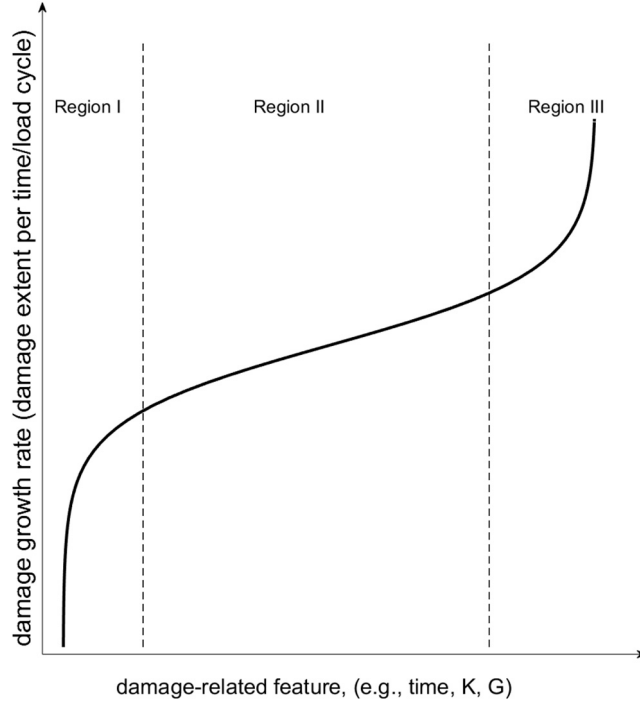$$x_k = x_{k-1} + C^*(\Delta K(x_{k-1}))^{m^*} e^\omega. \tag{14}$$

Fig. 2. Typical damage growth rate curve observed in structural degradation phenomena, in logarithmic scale. The first region is also called threshold or initiation region, the second region is the log-linear or stable propagation region and the third region is the critical or unstable propagation region.

The same noise was used in [20,21,29]. It was also used in [30] to estimate FCG using relevance vector machines. The multiplicative log-normal noise keeps the particles in the correct region of the state-space, because the log-normal distribution is defined in the positive region of real numbers. Then, it ensures that $x_k^{(i)} \geqslant x_{k-1}^{(i)} \, \forall i = 1, \ldots , N_s$. The tdf becomes a log-normal distribution with shift parameter x_{k-1}, (15),

$$p(x_k|x_{k-1}) = \frac{1}{(x_k - x_{k-1})\sigma_\omega\sqrt{2\pi}} \exp\left(-\frac{[\log(x_k - x_{k-1}) - \tilde{\mu}]^2}{2\sigma_\omega^2}\right),\tag{15}$$

where $\tilde{\mu} = \mu_\omega + \log\left(\frac{dx}{dN}\big|_{k-1}\right)$. Nonetheless, the zero-mean ω introduces a bias in the evolution equation and such a bias might generate an inefficient filter. The next paragraph explains why the log-normal distribution is a good choice for monotonic degradation processes, but also why the features of the log-normal distribution chosen in [19–21,29–31] introduced a bias that can be removed by the selection of a proper μ_ω.

Most of the structural damage progression models for aging or fatigue are based on power laws because of the (always) positive value of the damage growth rate, usually described by a nonlinear function similar to the one presented in Fig. 2. Crack length, delamination area (or length), and plastic deformation caused by creep are typical examples of damages undergoing to always-positive growth rate curves, so their severity can only increase as time passes by.

Common damage growth modeling approaches use the log-linear region (region II) to model the damage growth rate. By so doing, the estimation of the empirical model parameters requires only a simple linear regression, as shown in (16) for the estimation of C^* and m^* of the well-known Paris' law, in (17) for the estimation of A, B, α, β for composite damage modeling [26] and in (18) for the estimation of α and n of the Norton law for creep modeling, adopted in [32][2]:

$$\log\frac{dx}{dN} = \log C^* + m^* \log \Delta K + \omega,\tag{16}$$

$$\log\frac{dx}{dN} = \log A + \alpha \log \Delta G + \omega,$$
$$\log\frac{dx}{dN} = \log B + \beta \log \Delta G + \omega,\tag{17}$$

---

[2] The interested reader is referred to the original papers for details on the damage growth rate models presented here.

$$\log \frac{dx}{dt} = \log \alpha - \frac{\Phi}{RT} + n \log s + \omega. \tag{18}$$

The variable x above refers, generally, to some measure or feature of the damage extent. The term ω is the linear regression error, which is theoretically a zero-mean Gaussian variable, $\omega \sim \mathcal{N}(0, \sigma_\omega^2)$. The damage growth rates may be expressed by returning to the exponential form of the models reported in (19)–(21):

$$\frac{dx}{dN} = C^* (\Delta K)^{m^*} e^\omega, \tag{19}$$

$$\frac{dx}{dN} = A(\Delta G)^\alpha e^\omega, \tag{20}$$
$$\frac{dx}{dN} = B(\Delta G)^\beta e^\omega,$$

$$\frac{dx}{dt} = \alpha \exp\left(-\frac{\Phi}{RT}\right) s^n e^\omega. \tag{21}$$

As visible from (19)–(21), all the damage growth rate models have a multiplicative stochastic term e^ω, which is, by definition, log-normally distributed $e^\omega \sim \log\mathcal{N}(0, \sigma_\omega^2)$, [33]. However, a null mean value would introduce a bias in the conditional expectation of the damage growth rate, as proved hereafter.

Let us consider the conditional expected value of the evolution equation expressed through (22),

$$E[x_k | x_{k-1}] = x_{k-1} + E\left[\frac{dx}{dN}\bigg|_{k-1} e^\omega\right]. \tag{22}$$

Since e^ω is the only source of uncertainty, the product $dx/dN|_{k-1} e^\omega$ is log-normally distributed as well, (23),

$$\frac{dx}{dN}\bigg|_{k-1} e^{\omega_{k-1}} \sim \log\mathcal{N}\left(\mu_\omega + \log\frac{dx}{dN}\bigg|_{k-1}, \sigma_\omega^2\right). \tag{23}$$

Using the properties of the log-normal distribution [33], the expected value of the stochastic FCG rate can be written as in (24),

$$E\left[\frac{dx}{dN}\bigg|_{k-1} e^\omega\right] = e^{\mu_\omega} e^{\frac{\sigma_\omega^2}{2}} \exp\left(\log\frac{dx}{dN}\bigg|_{k-1}\right) = e^{\left(\mu_\omega + \frac{\sigma_\omega^2}{2}\right)} \frac{dx}{dN}\bigg|_{k-1}. \tag{24}$$

The expected value of the stochastic damage growth rate is the product of the mean of the log-normal term, $\exp(\mu_\omega + \sigma_\omega^2/2)$, and the deterministic damage growth rate $dx/dN|_{k-1}$. Thus, the selection of μ_ω and σ_ω^2 drives the expected value of the evolution equation. The random process $\omega \sim \mathcal{N}(0, \sigma_\omega^2)$ used in [19–21,29–31] produces a biased estimation of x_k, since $e^{\sigma_\omega^2/2} \neq 1 \; \forall \sigma_\omega^2 \in \mathbb{R}_{[0,\infty]}$. It introduces a *one-step prediction bias* ϵ_{x_k} between the stochastic and deterministic equation, quantifiable as the difference between the conditional expected value of the system state $E[x_k | x_{k-1}]$ and the deterministic evolution equation, (25):

$$\epsilon_{x_k} = E[x_k | x_{k-1}] - f_\theta'(x_{k-1})$$
$$= E\left[\frac{dx}{dN}\bigg|_{k-1} e^{\omega_{k-1}}\right] - \frac{dx}{dN}\bigg|_{k-1} = \frac{dx}{dN}\bigg|_{k-1} \left(e^{\left(\frac{\sigma_\omega^2}{2}\right)} - 1\right). \tag{25}$$

Intuitively, this bias increases when the prediction involves multiple steps $(k+1, k+2, \ldots)$. Also, the error is proportional to the noise variance σ_ω^2. This result is particularly important for the prognostic stage: if $\mu_\omega = 0$, the difference between the deterministic equation and the stochastic equation is directly proportional to both the length of the prediction and the variance σ_ω^2. A FCG simulation using the same mechanical properties reported in Table 2 and the process noise e^ω, $\omega \sim \mathcal{N}(0, \sigma_\omega^2)$ produced the propagations in Fig. 3. Therefore, the log-normal process noise with $\mu_\omega = 0$ has not been considered as a good perturbation source for particle filtering.

3.3. Definition of an optimal ω

The unbiased formulation of the evolution equation based on the multiplicative log-normal process noise may be easily obtained by selecting a mean value μ_ω that satisfies (26). Eq. (27) undergoes to such condition for any $\sigma_\omega^2 \in \mathbb{R}_{[0,\infty]}$,

$$E[e^\omega] = 1, \tag{26}$$
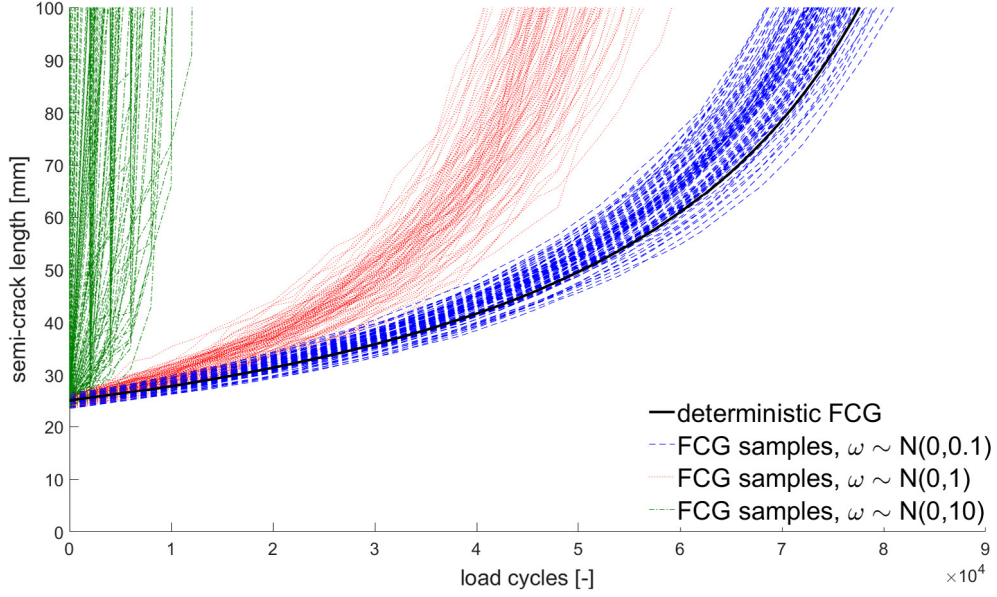
$$\mu_\omega = -\frac{\sigma_\omega^2}{2}. \tag{27}$$

Fig. 3. Monte Carlo simulation of FCG using the biased evolution equation and three values of σ_ω^2: 0.1, 1 and 10. The bias increases with the perturbation introduced by the process noise.

Fig. 4 shows the simulation of $N_s = 100$ FCGs, similar to the one presented in Figs. 1 and 3, using the process noise e^ω, $\omega \sim \mathcal{N}(-\sigma_\omega^2/2, \sigma_\omega^2)$. Fig. 4a, b, c and d refers to four different values of σ_ω^2. The swarm of particles in Fig. 4a, b and c appears always centered on the deterministic FCG simulation, without any effect on the mean value of the samples. The increasing variance introduces more and more perturbation in a single time step. If the variance becomes too large (Fig. 4d), most of the particles remain below the deterministic path (predicting a slower crack growth), and few particles remain above (predicting a faster and unlikely crack growth path), even if the expected value remains always equal to the deterministic model. The reason of this uneven distribution of the samples in the state-space is the asymmetry of the log-normal pdf, and can be avoided by selecting a reasonable σ_ω^2. Despite the drawback caused by the asymmetry of the distribution at relatively high σ_ω^2, the selection of the noise variance still remains independent on the closeness of the damage size to zero (a drawback affecting additive Gaussian noises), and a wide range of σ_ω^2 values can still provide satisfactory propagation of the particles. Such an unbiased evolution equation may also introduce further advantages on the selection of the sample size N_s. Since all the samples remain in the correct region of the state-space and they concentrate around plausible damage progression trajectories, a satisfactory approximation of the pdfs can be carried out with a reduced number of samples N_s, if compared with the sample size needed by other filters adopting a biased process noise.

3.4. Requirements for an unbiased and efficient evolution equation

The analysis of existing works has shown how additive Gaussian or multiplicative zero-mean log-normal distributions may cause systemic inaccuracies and computational difficulties for monotonic degradation monitoring. Therefore, a definition of some requirements that the evolution equation has to satisfy may help in designing an efficient algorithm:

- **support**: the random perturbation should not make the particles fall outside the domain support, otherwise the algorithm would waist computational power in propagating samples with null probability. Thus, the perturbation source has to guarantee that Eq. (28) holds.

$$x_k^{(i)} \subseteq \mathcal{X}, \ \forall k \in \mathbb{N}, i = 1, \dots, N_s \tag{28}$$

In the case of damage progression monitoring, the domain becomes $\mathcal{X} \in \mathbb{R}_{[0,\infty]}^{n \times 1}$.
- **monotonicity**: damage accumulation caused by fatigue or aging is inherently monotonic. The efficiency of the prognostic stage depends on the capability of the tdf to generate likely damage progression paths. Therefore, the tdf of the system state must guarantee that the samples increase during the one-step ahead transition, (29).

$$x_k^{(i)} \geqslant x_{k-1}^{(i)}, \ \forall k \in \mathbb{N}, i = 1, \dots, N_s \tag{29}$$
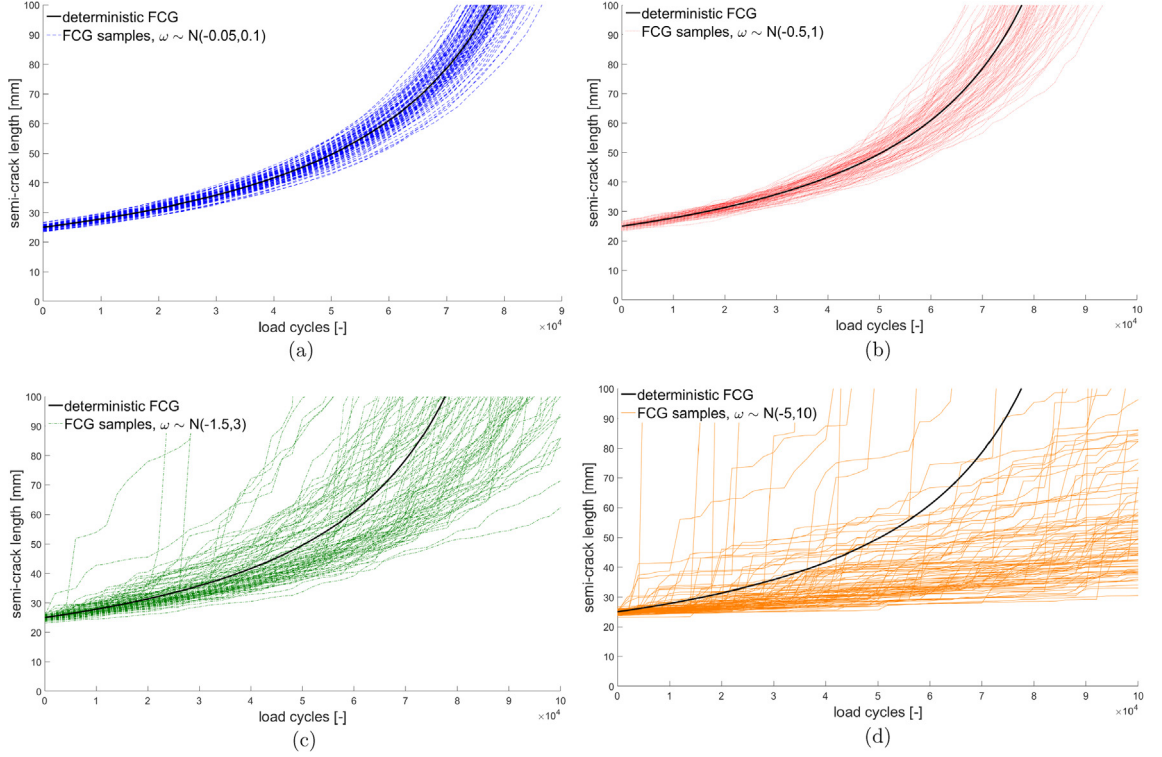
Fig. 4. FCG simulation using the unbiased evolution equation with log-Normal process noise using $\sigma_\omega^2 = 0.1$ (a), $\sigma_\omega^2 = 1$ (b), $\sigma_\omega^2 = 3$ (c) and $\sigma_\omega^2 = 10$ (d).

- **bias**: The random perturbation should not modify the particle trend, so it should not introduce biases in the evolution equation. Otherwise, to change the amount of noise in the filter would mean to change the trend of the particles. This is in contrast with the authors' belief that long-term drifts should be driven by the updating of the model parameters rather than by a bias induced by the process noise. The process noise should be the source of short-term random perturbations only, i.e. it should model the *intra-specimen* variability [34]. Thus, the tdf of the system state must satisfy (30),

$$\mathrm{E}[x_k|x_{k-1}] = f'_{\boldsymbol{\theta}}(x_{k-1}), \, \forall k \in \mathbb{N}. \tag{30}$$

The log-normal process noise that has been proposed here satisfies the three requirements discussed above. Then, the simulation of the damage progression may be easily addressed by using Eq. (31), where r is a sample from $\mathcal{N}(0, 1)$,

$$x_k = x_{k-1} + \frac{\mathrm{d}x}{\mathrm{d}N}\bigg|_{x_{k-1}} \exp\left(-\frac{\sigma_\omega^2}{2} + \sigma_\omega r\right). \tag{31}$$

4. Application to fatigue crack growth prediction

FCG data coming from a full-scale test of an aeronautical structure are used to validate the proposed algorithm against the existing formulations. The relevant features of the full-scale test are provided hereafter. Then, the section discusses the algorithm prognostic performances using dedicated metrics.

4.1. Full-scale FCG test on a helicopter tail

The tail of a retired Mi-8/17 helicopter is used as case-study. The full-scale FCG test was conducted in a lab environment as part of a European research project on SHM systems. A fatigue load was applied at the end of the tail to generate cyclic stresses in the material and induce crack initiation and propagation. The root of the tail was clamped to a rigid structure through a fiber-reinforced polymer component designed to simulate the stiffness of the central fuselage. The structure carrying the tail rotor was removed and the tail free-end was rigidly connected to an actuator. The applied force was perpendicular to the tail axis, and an offset between the force application point and the tail axis guaranteed the generation of both bending and torsion in the structure. Several local sensors and sensor networks were installed on the structure to monitor

the overall integrity of the tail and the crack progression as well. Though, data from the sensors have not been used here. The test required dedicated studies with finite element models for the test rig design and to evaluate the stress field of the tail during damage evolution [35]. The test rig is visible in Fig. 5, while the features of the FCG test are reported in Table 3.

An artificial notch was generated at a rivet hole in the region subject to positive normal stresses. The crack nucleated from the notch and propagated until the semi-crack length was around 35 mm, when the test was stopped. Fig. 6 shows a picture of the crack nucleation point, on the tip of the artificial notch. Once the crack was detected, it was repeatedly measured with a caliper during its propagation, and the measured semi-crack length has been used as input of the prognostic unit based on a particle filter. The resulting FCG is reported in Fig. 7. The crack nucleation needed around 400,000 load cycles, and then the crack propagated in $1 \cdot 10^6$ load cycles from 7.5 mm (the semi-length of the notch) up to 35 mm.

4.2. Remaining life prediction using particle filtering

A particle filtering-based prognostic unit has been developed to monitor the crack growth evolution and predict when the semi-crack length x reached the final size, which is $x_f = 36.2$ mm, after $N_f = 1.385 \cdot 10^6$ load cycles. After the first measure of the semi-crack length, the other measures were provided to the algorithm sequentially, thus simulating a real time condition. The measurement system has been modeled as unbiased and Gaussian, with fixed variance $\sigma_\eta^2 = 1$ mm^2. The model underneath the filter is Paris' law with the analytical formulation of the stress intensity factor as done for the simulation in Section 3. The remote stress S was estimated by a finite element model of the structure, [35]. The particle filtering algorithm is a *sequential importance resampling* with systematic resampling [3], and a *kernel smoothing* sub-algorithm [36] has been used to update the model parameters during run-time. Such updating of the model parameters, which has not been discussed herein, improves the prediction capability of the filter without affecting the process noise selection. Model parameter updating and process noise should be treated separately as their objective is, as a matter of fact, decoupled. The goal of real-time parameter updating is to refine the underneath model conditional on the observed data, thus aiming at improving the prediction of future trends. On the other hand, the process noise is instead a representation of non-modelled phenomena and variabilities of true dynamic processes that are not accounted for in typical engineering models. The random perturbation introduced by the process noise should not significantly modify the trend of the particle swarm, the latter being the goal of the model parameter updating procedure, while it should enlarge or shrink the particle dispersion. In this application, the model parameter vector composes of the two Paris' law parameters, $\theta = [\log C^*, m^*]^T$. The logarithmic form of C^* should be
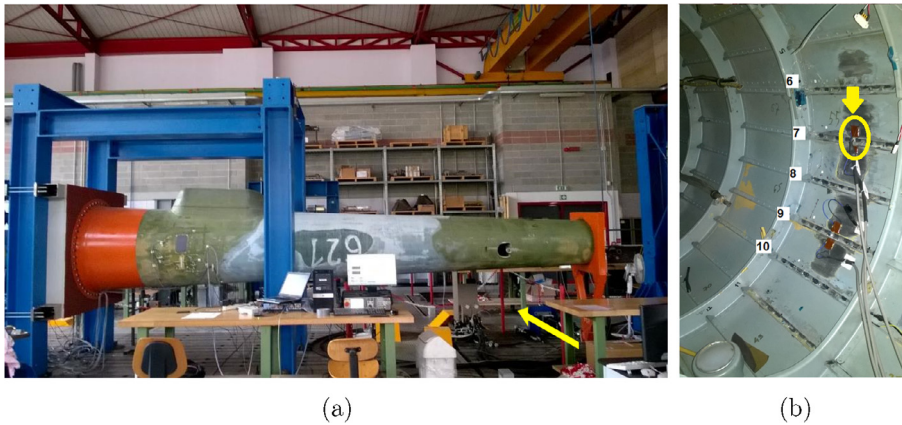

Fig. 5. Full-scale FCG test on the Mi-8/17 helicopter tail (a) and most stressed region with a FBG-based sensor network on the inner stringers (b). The thick arrow on bottom-right of (a) shows the load direction, applied through a hydraulic actuator, while the circle in (b) shows the crack nucleation point from a rivet hole.

Table 3
full-scale FCG test features.

Load shape	Sinusoidal
Load frequency	1 Hz
Maximum load	8 kN
Load ratio (R)	0.1
Damage type	Skin crack
Damage location	Rivet hole
Damage initiation	Artificial notch, 15 mm
Skin material (driving FCG)	D-16 (equivalent to Al2024-T4)

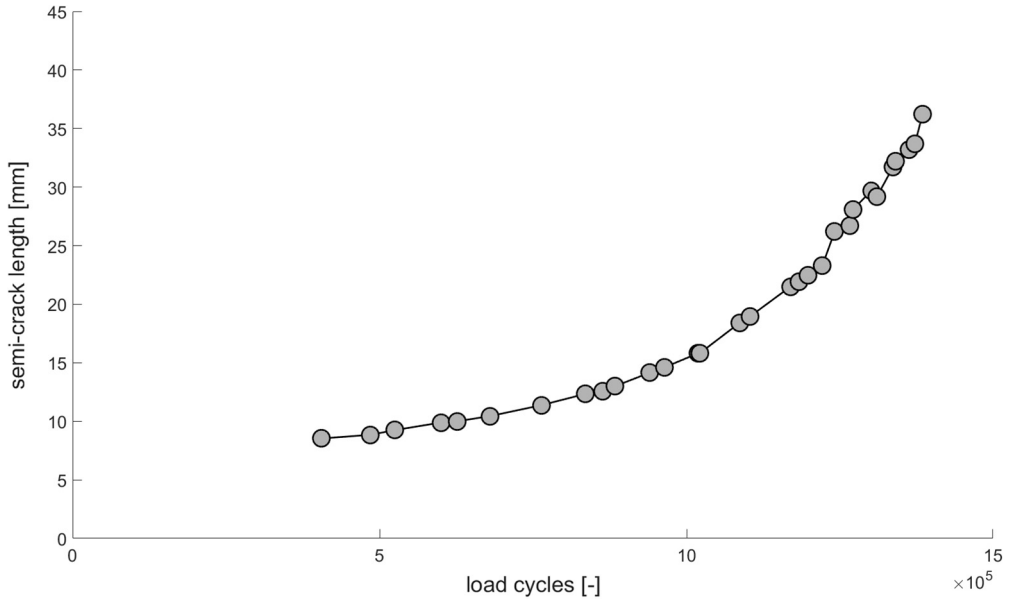**Fig. 6.** Crack nucleation from the notch at the rivet hole.

Fig. 7. Semi-crack length against fatigue load cycles.

noted, since it is log-normally distributed [37,34]. The initialization of the model parameters follows the historical data of the Al2024-T3 aluminum alloy studied by Virkler, Hillberry and Goel, [38]

$$
\begin{aligned}
&\boldsymbol{\theta}_0 \sim \mathcal{N}(\boldsymbol{\mu}_{\theta,0}, \boldsymbol{\Sigma}_{\theta,0}), \\
&\boldsymbol{\mu}_{\theta,0} = [\log(1.994 \cdot 10^{-14}), 3.79]^T, \\
&\boldsymbol{\Sigma}_{\theta,0} = \begin{bmatrix} 0.9966 & -0.1764 \\ -0.1764 & 0.0346 \end{bmatrix}.
\end{aligned}
\tag{32}
$$

Eqs. (33) and (34) represent the evolution equation for the *i-th* sample using the multiplicative log-normal and the additive process noise, respectively.

$$x_k^{(i)} = x_{k-1}^{(i)} + \left.\frac{dx}{dN}\right|_{\mu_{\theta,k}^{(i)}} \Delta N e^{\omega^{(i)}},$$

$$\theta_k^{(i)} = \tilde{\mu}_{\theta,k}^{(i)} + \mathcal{N}(0, h^2 V[\theta]_{k-1}),$$

(33)

$$x_k^{(i)} = x_{k-1}^{(i)} + \left.\frac{dx}{dN}\right|_{\mu_{\theta,k}^{(i)}} \Delta N + \omega^{(i)},$$

$$\theta_k^{(i)} = \tilde{\mu}_{\theta,k}^{(i)} + \mathcal{N}(0, h^2 V[\theta]_{k-1}).$$

(34)

The evolution equation (eq. (33) or (34)) and the observation equation in (35) form the dynamic state-space model of the system,

$$z_k \sim \mathcal{N}(x_k, \sigma_\eta^2).$$

(35)

The term $\tilde{\mu}_{\theta,k}^{(i)}$ is the *i-th* kernel location evaluated with the shrinkage rule from West [39,40], and follows (36),

$$\tilde{\mu}_{\theta,k}^{(i)} = b\,\theta_{k-1}^{(i)} + (1-b)\,E[\theta]_{k-1},$$

(36)

where $b = \sqrt{1 - h^2}$ and $h \in [0,1]$ is the smoothing parameter, a choice of the algorithm designer [36]. In this application, the smoothing parameter has been kept equal to $h = 0.1$ for all the simulations, and $\Delta N = 500$. The two moments $E[\theta]_{k-1}$ and $V[\theta]_{k-1}$ are the Monte Carlo-mean and -variance of the model parameters at the previous time step, respectively.

4.3. Analysis of prediction results

A RUL prediction is made for every measure of the semi-crack length. The predictions made with different algorithms (i.e., particle filters with different process noises) are compared below. The initial distributions of the process noise have been selected empirically to guarantee satisfactory results, and their values are available in Table 4. Then, they have been increased at each run to assess the robustness of the algorithms. All the runs presented below have a sample size of $N_s = 600$, which has been considered enough to correctly represent the pdfs involved in the filtering process.

The performance of the algorithm has been validated using the percentage error and dedicated prognostic metrics proposed in [41]: prognostic horizon (PH), $\alpha\lambda$ accuracy (AL), cumulative relative accuracy (CRA) and convergence (CN) have been selected to compare the results of the algorithm against increasing values of the noise pdf parameters. The definition of such metrics has been slightly modified from [41] and adapted to this specific application.

- **Prognostic horizon** 'is the difference between the current time index k and the end-of-prediction utilizing data accumulated up to the time index, provided the prediction meets desired specifications', [41]. In this application, the end-of-prediction is the end of the test, so the number of load cycles N_f, and the PH is the number of load cycles when 60% of the RUL distribution first falls within the range RUL $\pm$ 10%N_f. Also, the PH has been divided by the *time of prediction*: $N_f - N_{k,0}$, where $N_{k,0}$ is the number of load cycles at the first prediction. By doing so, the PH can be compared with PH values obtained from other data or runs, characterized by a different time of prediction.
- **$\alpha\lambda$ accuracy** 'is the prediction accuracy at specific time instances, usually defined as the demand accuracy of prediction to be within $\alpha 100\%$ after a specific time instant', [41]. In this application, the $\alpha\lambda$ accuracy is the number of times that 60% of the RUL distribution falls within a region that shrinks as time passes by. This region begins when the PH requirement has first been met, and has the shape of a triangle that shrinks with the load cycles in the RUL plot.
- **Cumulative relative accuracy** 'is the normalized sum of relative accuracy (RA) at specific time instances' [41], (37),

$$\text{CRA} = \sum_{j=1}^{k'} \gamma_j \text{RA}_j.$$

(37)

Table 4

Initial noise pdf parameters. The mean value $\mu_\omega = 0$ for the normal and log-normal process noises, except for the unbiased log-normal.

Noise type	Noise pdf parameters
Additive, Gamma	$k_0^* = 1.5 \cdot 10^{-3}$, $\theta_0^* = 3 \cdot 10^{-3}$
Additive, normal	$\sigma_{\omega,0}^2 = 1 \cdot 10^{-4}$
Multiplicative, log-normal	$\sigma_{\omega,0}^2 = 0.1$
Unbiased, log-normal	$\sigma_{\omega,0}^2 = 0.1$

The term k' is the number of predictions (corresponding to the number of observations of the semi-crack length) during the entire time of prediction (i.e., $k = 0, \ldots, k'$). The terms γ_j are weights, which can be arbitrarily selected. Here, They linearly increase from 0 to 1 with j, so a prediction error in the final stage of the prognosis (i.e., when the system is approaching its end-of-life) is penalized with respect to a prediction error in the early stage (i.e., when the prognostic
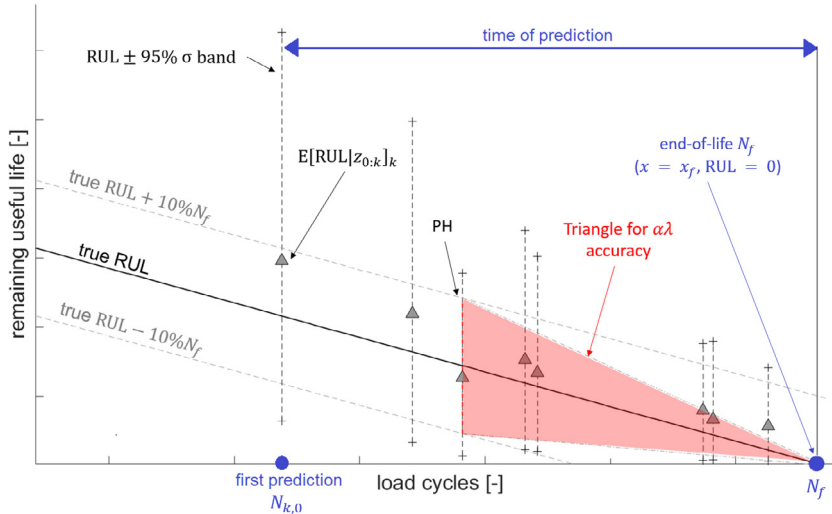

Fig. 8. Example of RUL plot emphasizing relevant features for the prognostic performance assessment.
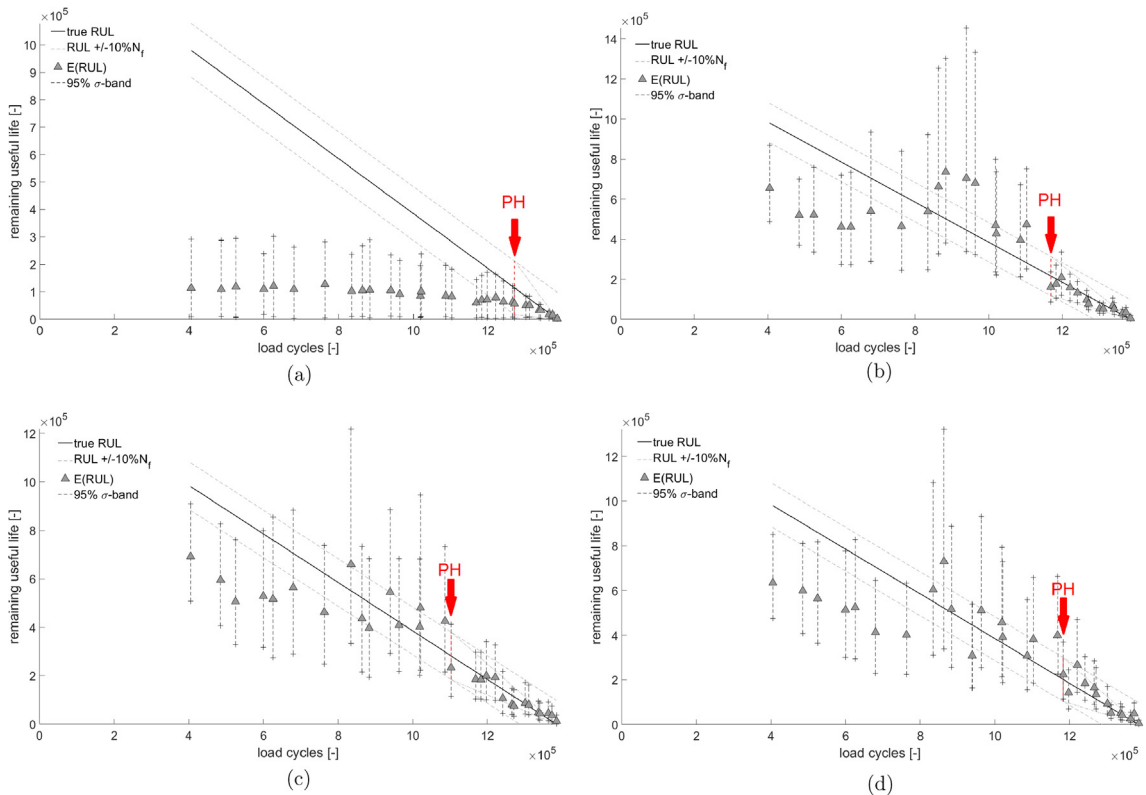
Fig. 9. RUL predictions using different process noises with features presented in Table 4. Additive Gamma process (a), additive Gaussian (b), multiplicative, biased log-normal (c) and multiplicative, unbiased ('optimal') log-normal (d). The thick arrows indicate the instant when the PH requirement has first been met.

process is just started and the algorithm has collected a few data). It should be noticed that $\sum_j \gamma_j = 1$. The RA is defined as the reciprocal of the relative error, (38),

$$RA_k = 1 - \frac{|RUL_k - E[RUL|z_{0:k}]_k|}{RUL_k}.$$ (38)

- **Convergence** 'is defined to quantify the manner in which any metric improves with time', [41]. The CN is estimated as the center of mass of the area under the metric curve. In this application, the CN has been evaluated using the relative error, which is the second addendum of the right hand-side of (38). As already made for the PH, the convergence has been divided by the time of prediction. The interested reader is referred to [41] for the estimation of the CN.

Fig. 8 shows some relevant features of the RUL estimation plot. In this application, the RUL is the number of load cycles to reach the final crack length $x_{th} = x_f$. Besides PH and $\alpha\lambda$ accuracy, Fig. 8 shows the features to estimate the most relevant prognostic metrics as highlighted by the work of Saxena et al. [41]. The time of prediction is defined as the time between the first RUL prediction, defined as first prediction in the figure, and the end of life. The constant confidence band around the true RUL is used to define the other prognostic metrics, i.e., PH and $\alpha\lambda$ accuracy. Since such a confidence band is defined here as a function of the end of life, it can be evaluated after the end of test, once the true N_f is available. The grey triangles are the expected values of the RUL conditioned on the observed measurements, and the dashed vertical grey lines represent the σ-band of the predicted RUL. The lower and upper limits of the *sigma*-band are estimated from the cumulative distribution function of the RUL, approximated by the particle set, by respectively finding $RUL_k^* : \Pr\{RUL_k \leqslant RUL_k^*\} = \alpha$ and $RUL_k^{**} : \Pr\{RUL_k \leqslant RUL_k^{**}\} = 1 - \alpha$, with $\alpha = 0.025$ to obtain a 95%σ-band. Those features and the other metrics presented above have been used to evaluate the performance of the prognostic algorithm.

Each algorithm has been run using the process noise models in Table 4, and the results are summarized in Fig. 9. As seen in Fig. 9a, the additive Gamma process noise introduces a large bias in the particle swarm, insomuch as the RUL prediction capabilities are strongly reduced. This result could be improved by adopting much smaller values of the Gamma pdf moments, so much smaller k^* and θ^*. However, such choice would be, as thoroughly discussed in Section 3, strongly case-sensitive. Also, a too small of value for the Gamma pdf parameters may vanish the perturbation effect of the process noise. The other formulations produce much better results, and their predictions are comparable to one another (Fig. 9b–d). However, these results change with the process noise pdf parameters, as is shown below.

The performance of the prediction has been evaluated using a different amount of process noise, which has been increased using the following sequence: 1, 2, 5, 10, 20, 50, 80 and 100 times the original value. This means that the process
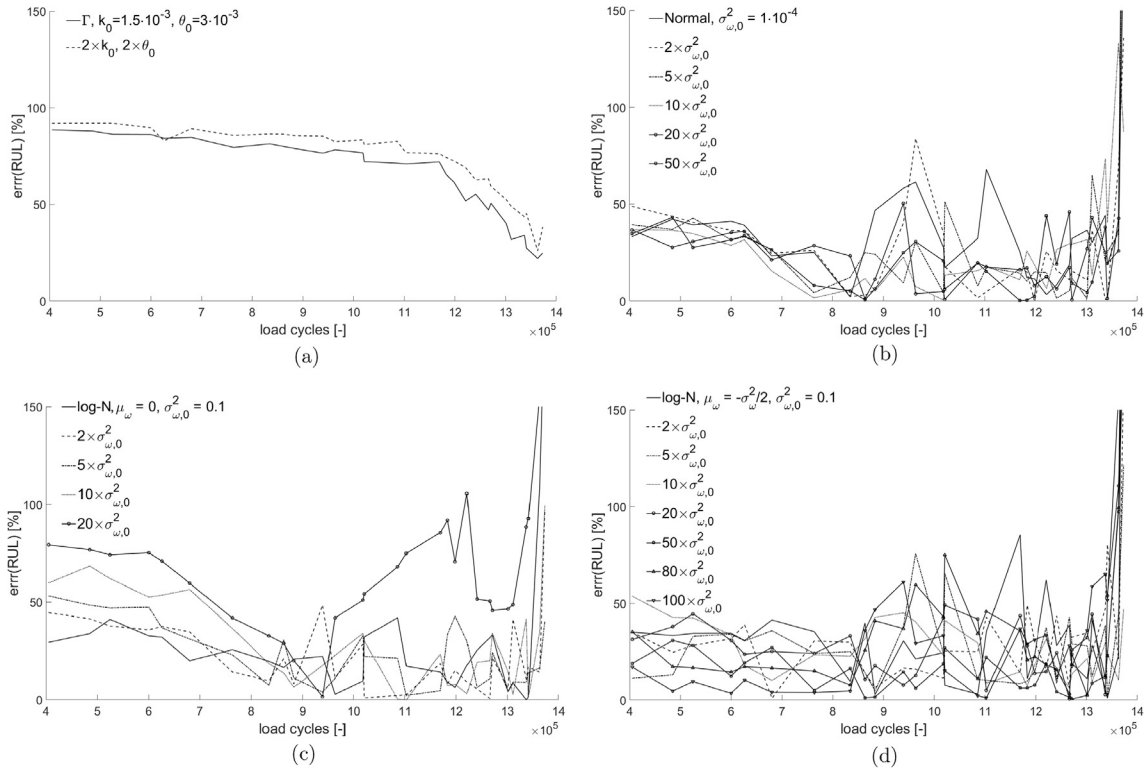

Fig. 10. Percentage error of the RUL prediction using increasing process noise moments: Gamma pdf (a), Gaussian pdf (b), log-normal pdf, biased noise (c) and log-normal pdf, unbiased ('optimal') noise (d).

noise parameters have been multiplied by 1, 2, 5, etc. and the RUL prediction performance has been evaluated for each run. The percentage error of the RUL prediction is presented in Fig. 10. The algorithm using the Gamma process noise model fails when the Gamma pdf parameters are larger that 2 times the initial k_0^*, θ_0^*. Then, only two curves are visible in Fig. 10a. The percentage error remains high during the entire simulation, and the additional information on the semi-crack length does not help in increasing the accuracy of the prediction. The error eventually decreases during the last part of the test. The normal process noise model shows a smaller percentage error, which appear insensitive to σ_ω^2 (Fig. 10b). The percentage error remain slightly below 50% up to $8 \cdot 10^5$ load cycles, independently from the process noise variance. Also, the algorithm is not able to converge at all when the process noise variance becomes too large, because some (or, at least, one) particles fall below zero, thus never reaching x_f. Therefore, the curves refer to variances $\sigma_{\omega,0}^2, \ldots, 50 \cdot \sigma_{\omega,0}^2$. The biased log-normal process noise model (Fig. 10c) shows a percentage error that increases with the amount of variance σ_ω^2, and the algorithm does not converge when such variance enlarges ($\sigma_\omega^2 > 20 \cdot \sigma_{\omega,0}^2$). The failure of this algorithm is caused by the fast propagation of the particles. When σ_ω^2 becomes too large, many particles fail in a single propagation step, thus not providing any RUL prediction. On the contrary, the algorithm based on the unbiased log-normal process noise model converges for all of the tested variances, $\sigma_{\omega,0}^2, \ldots, 100 \cdot \sigma_{\omega,0}^2$. The percentage error is slightly different at each run (i.e., with different σ_ω^2), but is not proportional to σ_ω^2.

Fig. 11 shows the four metrics assessed against the process noise pdfs. These metrics confirm the robustness indicated by the percentage error. The PHs of the algorithm with $\omega \sim \Gamma(k^*, \theta^*)$ are significantly lower than the PHs observed with other algorithms and, as remarked above, the algorithm converges only when $k^* \leqslant 2 \cdot k_0, \theta^* \leqslant 2 \cdot \theta_0$. Except for the case $\bar{\sigma}_\omega = 5 \cdot \sigma_{\omega,0}$, the algorithms with Normal and log-Normal process noises show similar prognostic horizons. Nevertheless, the unbiased log-normal model always converges, even when the variance σ_ω^2 is two orders of magnitude larger than the initial one. The analysis of the AL, CRA and CN yields similar conclusions. It is worth noting that the high AL values obtained with the Gamma process noise have been caused by the very short PH and the narrow RUL pdf. As a matter of fact, AL and PH discussed here are strongly correlated, so high AL does not guarantee good prognostic capabilities. AL and PH should be analyzed together. All the plots in Fig. 11 shows that the performance of the unbiased log-Normal slightly decrease when σ_ω^2 becomes very large with respect to the initial value ($\sigma_\omega^2 \geqslant 80 \cdot \sigma_{\omega,0}^2$). This small drop in the performance may be caused by the asymmetry of the log-normal distribution, as presented in Section 3, Fig. 4. According to the results discussed above, the algorithm based on the unbiased log-normal process noise can be considered more robust with respect to other
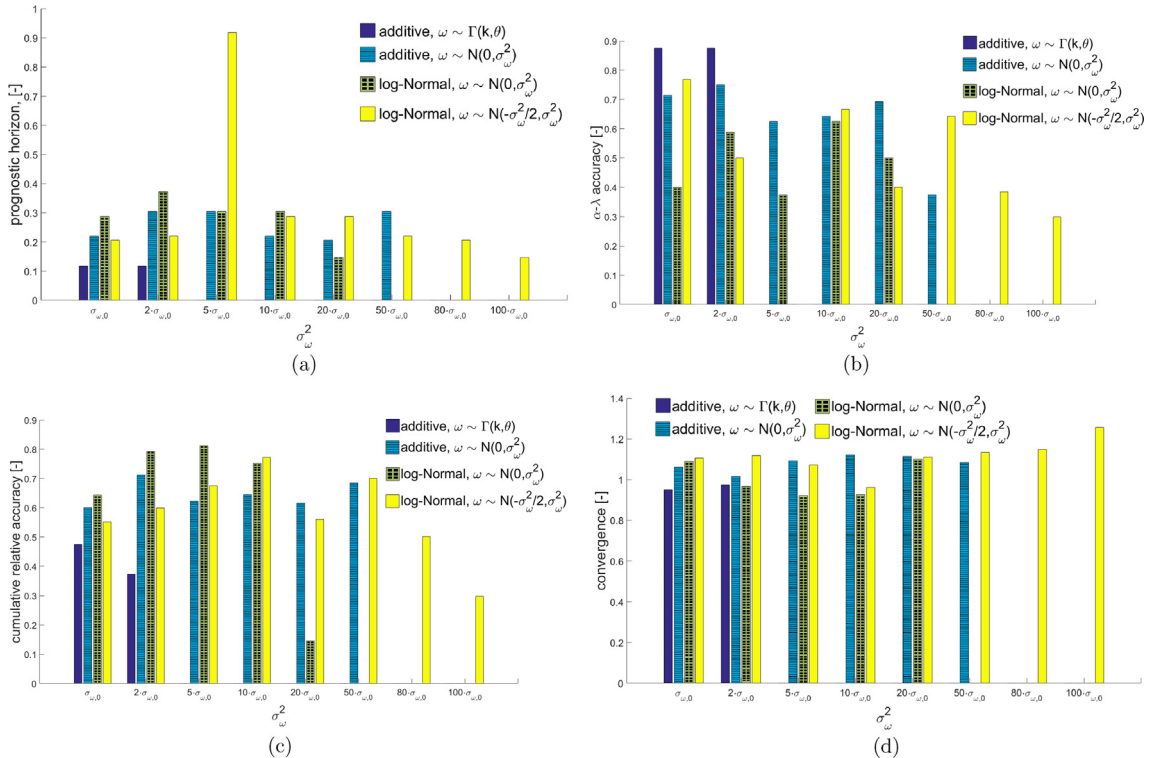

Fig. 11. Prognostic horizon (a), $\alpha\lambda$ accuracy (b), cumulative relative accuracy (c) and convergence (d) of the four algorithms as a function of the process noise parameters.

formulations presented in literature. The selection of a very large variance σ_ω^2 could affect the algorithm performance, but the prognostic unit will always converge regardless to the entity of the perturbation introduced with the random process.

5. Conclusions

The work reported herein has analyzed the process noise adopted in a typical Bayesian filtering algorithm for nonlinear, non-Gaussian systems. The paper discussed the particle filtering capabilities to predict the evolution of monotonic degradation processes with respect to the type of process noise, specifically analyzing the case of structural damage progressions caused by aging or fatigue. The conditional expectation of the system state has shown that some process noise formulations, already adopted in literature, might cause inefficiency in the algorithm. Also, the algorithm might not even converge if the samples fall outside of the state-space or the bias between the stochastic and deterministic equation becomes too large. This analysis has brought to an unbiased evolution equation grounding on a log-normal process noise with a specific constraint imposed between its mean and variance, and also to three requirements that the design of the filter has to meet to guarantee the efficiency and effectiveness of the diagnostic/prognostic process.

The proposed particle filtering and the other existing formulations from literature have been tested on FCG observed in a full-scale helicopter tail subject to tension-tension fatigue loads. The results have been compared in terms of RUL prediction error and four performance metrics: PH, AL, CRA and CN. The results emphasized the robustness of the proposed algorithm against the other formulations. Furthermore, the results suggest that the additive Gaussian (with zero mean) and the proposed unbiased log-normal process noise have comparable performance, but the filter based on the additive Gaussian noise may fail when the variance becomes too large. The variance selection problem of the additive Gaussian noise can be easily addressed when the system state is unidimensional like the semi-crack length discussed in this paper, but could become non-trivial for multidimensional system states or more complex system dynamics. Therefore, the unbiased log-normal process noise proposed here has been considered the best choice to monitor and predict monotonic degradation processes.

The selection of the process noise variance magnitude has not been addressed in this paper. Its optimal value depends, among other factors, from the uncertainty of the observations, and how widespread they are in the state-space. Therefore, a discussion on the process noise variance magnitude would involve the uncertainty characterizing the observation equation. Future research should target the identification of quantitative probabilistic methods to select this fundamental particle filtering parameter. Also, further research on the topic may discuss optimal process noise models to monitor and predict the evolution of other types of degradation phenomena at component- or system-level.

Acknowledgments

References

[1] N.J. Gordon, D.J. Salmond, A.F. Smith, Novel approach to nonlinear/non-Gaussian bayesian state estimation 140(2) (1993) 107–113.
[2] A. Doucet, S. Godsill, C. Andrieu, On sequential monte carlo sampling methods for bayesian filtering, Stat. Comput. 10 (3) (2000) 197–208.
[3] M.S. Arulampalam, S. Maskell, N. Gordon, T. Clapp, A tutorial on particle filters for online nonlinear/non-gaussian bayesian tracking, IEEE Trans. Signal Process. 50 (2) (2002) 174–188.
[4] Z. Chen, Bayesian filtering: from kalman filters to particle filters, and beyond, Statistics 182 (1) (2003) 1–69.
[5] A. Haug, A Tutorial on Bayesian Estimation and Tracking Techniques Applicable to Nonlinear and Non-Gaussian Processes, MITRE Corporation, McLean.
[6] J. Ching, J.L. Beck, K.A. Porter, Bayesian state and parameter estimation of uncertain dynamical systems, Probab. Eng. Mech. 21 (1) (2006) 81–96.
[7] S. Xue, H. Tang, Q. Xie, Structural damage detection using auxiliary particle filtering method, Struct. Health Monit. 8 (2) (2009) 101–112.
[8] M. Compare, P. Baraldi, P. Turati, E. Zio, Interacting multiple-models, state augmented particle filtering for fault diagnostics, Probab. Eng. Mech. 40 (2015) 12–24.
[9] P. Baraldi, F. Cadini, F. Mangili, E. Zio, Model-based and data-driven prognostics under different available information, Probab. Eng. Mech. 32 (2013) 66–79.
[10] B. Saha, K. Goebel, S. Poll, J. Christophersen, An integrated approach to battery health monitoring using bayesian regression and state estimation, in: Autotestcon, 2007 IEEE, IEEE, 2007, pp. 646–653.
[11] K. Goebel, B. Saha, A. Saxena, J.R. Celaya, J.P. Christophersen, Prognostics in battery health management, IEEE Instrum. Meas. Mag. 11 (4) (2008) 33.
[12] J. Chiachío, M. Chiachío, S. Sankararaman, A. Saxena, K. Goebel, Condition-based prediction of time-dependent reliability in composites, Reliab. Eng. Syst. Safety (2015) 134–147.
[13] E. Chatzi, A.W. Smyth, Nonlinear system identification: particle based methods, Encyclopedia of Earthquake Engineering: SpringerReference.
[14] A. Oliver, A.W. Smyth, Particle filtering and marginalization for parameter identification in structural systems, Struct. Control Health Monit. 24 (3) (2017).
[15] M.E. Orchard, G.J. Vachtsevanos, A particle filtering approach for on-line failure prognosis in a planetary carrier plate, Int. J. Fuzzy Logic Intell. Syst. 7 (4) (2007) 221–227.
[16] M.E. Orchard, G.J. Vachtsevanos, A particle filtering-based framework for real-time fault diagnosis and failure prognosis in a turbine engine, in: Mediterranean Conference on Control & Automation, 2007. MED'07, IEEE, 2007, pp. 1–6.
[17] M. Orchard, G. Kacprzynski, K. Goebel, B. Saha, G. Vachtsevanos, Advances in uncertainty representation and management for particle filtering applied to prognostics, in: International Conference on Prognostics and Health Management, 2008. phm 2008, IEEE, 2008, pp. 1–6.

[18] M.E. Orchard, G.J. Vachtsevanos, A particle-filtering approach for on-line fault diagnosis and failure prognosis, Trans. Inst. Meas. Control 31 (3–4)(2009) 221–246.
[19] F. Cadini, E. Zio, D. Avram, Monte carlo-based filtering for fatigue crack growth estimation, Probab. Eng. Mech. 24 (3) (2009) 367–373.
[20] F. Cadini, E. Zio, D. Avram, Model-based monte carlo state estimation for condition-based component replacement, Reliab. Eng. Syst. Safety 94 (3) (2009) 752–758.
[21] E. Zio, G. Peloni, Particle filtering prognostic estimation of the remaining useful life of nonlinear components, Reliab. Eng. Syst. Safety 96 (3)(2011) 403–409.
[22] D. An, J.-H. Choi, N.H. Kim, Prognostics 101: a tutorial for particle filter-based prognostics algorithm using matlab, Reliab. Eng. Syst. Safety 115 (2013) 161–169.
[23] P. Baraldi, M. Compare, S. Sauco, E. Zio, Ensemble neural network-based particle filtering for prognostics, Mech. Syst. Signal Process. 41 (1) (2013) 288–300.
[24] J. Chiachío, M. Chiachío, A. Saxena, G. Rus, K. Goebel, An energy-based prognostics framework to predict fatigue damage evolution in composites, in: Proceedings of the Annual Conference of the Prognostics and Health Management Society, vol. 1, 2013, pp. 363–371.
[25] M. Chiachío, J. Chiachío, A. Saxena, G. Rus, K. Goebel, An efficient simulation framework for prognostics of asymptotic processes-a case study in composite materials, in: Proceedings of the European Conference of the Prognostics and Health Management Society, Nantes, France, 2014, pp. 202–214.
[26] M. Corbetta, C. Sbarufatti, M. Giglio, S. Abhinav, K. Goebel, Model-based fatigue prognosis of fiber-reinforced laminates exhibiting concurrent damage mechanisms, in: 6-th European Conference on Structural Control, 2016, pp. –.
[27] M. Jouin, R. Gouriveau, D. Hissel, M.-C. Péra, N. Zerhouni, Particle filter-based prognostics: review, discussion and perspectives, Mech. Syst. Signal Process. 72–73 (2016) 2–31.
[28] G.C. Sih, J. Provan, Probabilistic Fracture Mechanics and Reliability, vol. 6, Springer Science & Business Media, 2013.
[29] W. Yang, S. Yuan, L. Qiu, H. Zhang, B. Ling, A particle filter and lamb wave based on-line prognosis method of crack propagation in aluminum plates, in: 4th International Symposium on NDT in Aerospace, 2012.
[30] E. Zio, F. Di Maio, Fatigue crack growth estimation by relevance vector machine, Exp. Syst. Appl. 39 (12) (2012) 10681–10692.
[31] E. Zio, F. Di Maio, A data-driven fuzzy approach for predicting the remaining useful life in dynamic failure scenarios of a nuclear system, Reliab. Eng. Syst. Safety 95 (1) (2010) 49–57.
[32] P. Baraldi, F. Mangili, E. Zio, A kalman filter-based ensemble approach with application to turbine creep prognostics, IEEE Trans. Reliab. 61 (4)(2012) 966–977.
[33] D.C. Montgomery, G.C. Runger, N.F. Hubele, Engineering Statistics, John Wiley & Sons, 2009.
[34] J.M. Bourinet, M. Lemaire, Form sensitivities to correlation: application to fatigue crack propagation based on virkler data, in: 4th International ASRANet Colloquium, 2008.
[35] C. Sbarufatti, M. Corbetta, J. Sanmillan, M. Frovel, M. Stefaniuk, M. Giglio, Model-assisted performance qualification of a distributed shm system for fatigue crack detection on a helicopter tail boom, in: 8th European Workshop on Structural Health Monitoring, EWSHM 2016 - 3rd European Conference of the Prognostics and Health Management (PHM) Society, 2016.
[36] J. Liu, M. West, Combined parameter and state estimation in simulation-based filtering, in: Sequential Monte Carlo methods in Practice, Springer, 2001, pp. 197–223.
[37] Z.A. Kotulski, On efficiency of identification of a stochastic crack propagation model based on virkler experimental data, Arch. Mech. 50 (5) (1998) 829–847.
[38] D. Virkler, B. Hillberry, P. Goel, The statistical nature of fatigue crack propagation, J. Eng. Mater. Technol. 101 (2) (1979) 148–153.
[39] M. West, Mixture models, monte carlo, bayesian updating, and dynamic models, Comput. Sci. Stat. (1993), pp. 325–325.
[40] M. West, Approximating posterior distributions by mixture, J. Roy. Stat. Soc. Ser. B (Methodol.) (1993) 409–422.
[41] A. Saxena, J. Celaya, E. Balaban, K. Goebel, B. Saha, S. Saha, M. Schwabacher, Metrics for evaluating performance of prognostic techniques, in: International Conference on Prognostics and Health Management, 2008. phm 2008, IEEE, 2008, pp. 1–17.